JACS
JOURNAL OF THE AMERICAN CHEMICAL SOCIETY
Article
pubs.acs.org/JACS

Engineering Topochemical Polymerizations Using Block Copolymer Templates

Liangliang Zhu,[†] Helen Tran,[†] Frederick L. Beyer,[‡] Scott D. Walck,[‡] Xin Li,[§] Hans Ågren,[§] Kato L. Killops,*[,∥] and Luis M. Campos*[,†]

[†]Department of Chemistry, Columbia University, New York, New York 10027, United States
[‡]Army Research Laboratory, Aberdeen Proving Ground, Maryland 21005, United States
[§]Division of Theoretical Chemistry and Biology, School of Biotechnology, KTH Royal Institute of Technology, SE-10691 Stockholm, Sweden
[∥]Edgewood Chemical Biological Center, Aberdeen Proving Ground, Maryland 21010, United States

Supporting Information

ABSTRACT: With the aim to achieve rapid and efficient topochemical polymerizations in the solid state, via solution-based processing of thin films, we report the integration of a diphenyldiacetylene monomer and a poly(styrene-*b*-acrylic acid) block copolymer template for the generation of supramolecular architectural photopolymerizable materials. This strategy takes advantage of non-covalent interactions to template a topochemical photopolymerization that yields a polydiphenyldiacetylene (PDPDA) derivative. In thin films, it was found that hierarchical self-assembly of the diacetylene monomers by microphase segregation of the block copolymer template enhances the topochemical photopolymerization, which is complete within a 20 s exposure to UV light. Moreover, UV-active cross-linkable groups were incorporated within the block copolymer template to create micropatterns of PDPDA by photolithography, in the same step as the polymerization reaction. The materials design and processing may find potential uses in the microfabrication of sensors and other important areas that benefit from solution-based processing of flexible conjugated materials.

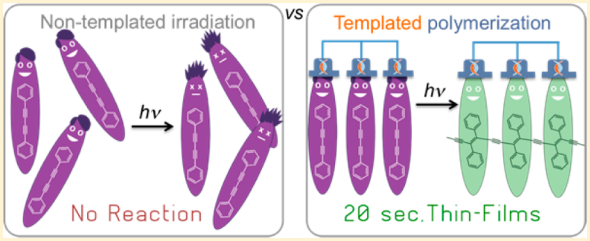

INTRODUCTION

Chemical transformations in constrained media have enabled grand technological advancements and a deep fundamental understanding of reaction mechanisms.[1−4] While unimolecular processes have less stringent requirements to engineer reactivity in the solid state,[5−9] bimolecular and polymerization reactions can be challenging.[10−13] In the latter case, preorganization of the reactive components is crucial, where bond-making and bond-breaking must occur with minimal atom displacement. To align the building blocks, these topochemical transformations are generally carried out in highly ordered systems, such as molecular cages,[14] monolayers,[15,16] nanoporous materials,[17] and crystals.[18−20] The ability to template topochemical reactions in amorphous media (such as polymers), however, has received little attention due to the lack of control of intermolecular alignment of the reactive species.[3] Interestingly, block copolymers (BCPs) can lead to ordered phases where appropriate functionalization yields close packing arrangements.[21] Thus, we sought to exploit the use of side-chain supramolecular BCP templates to investigate chemical reactivity in constrained media.

The seminal work by Wegner on the topochemical polymerization of diacetylene (DA) demonstrated that its molecular orientation was essential to react by 1,4-addition to yield polydiacetylene, a conjugated polymer.[22] With the growing interest for these materials to be exploited in excitonic photovoltaic devices (polydiacetylene undergoes singlet fission),[23] sensors,[24,25] bioelectronic materials,[26] and other optoelectronic devices,[27] the past decade has witnessed increased interest in controlling the polymerization of DAs. The key strategies have been based on grafting DA monomers on surfaces to form monolayers that are well-aligned[17] and introducing functional groups on the DA monomers to control their aggregation and crystallization, followed by thermal or photochemical polymerization.[18,28] The reactivity of such constructs is usually sluggish, where polymerization proceeds within minutes to hours by heating or UV light.[29,30] Recently, Shimizu and co-workers have shown that DA-containing macrocycles can crystallize with the appropriate arrangement for polymerization, though the reaction takes 3 h with heating.[31,32] Exploiting biomimetic supramolecular interactions, Tovar and co-workers found that the arrangement of diphenyldiacetylene (DPDA) monomers using oligopeptides can guide the supramolecular assembly, where photopolymerization occurs within 30 min to yield polydiphenyldiacetylene (PDPDA).[33] In all these cases, the polymerizations are system-specific and not amenable for thin-film processing. Solution-

Received: July 18, 2014
Published: September 11, 2014

dx.doi.org/10.1021/ja507318u | J. Am. Chem. Soc. 2014, 136, 13381−13387

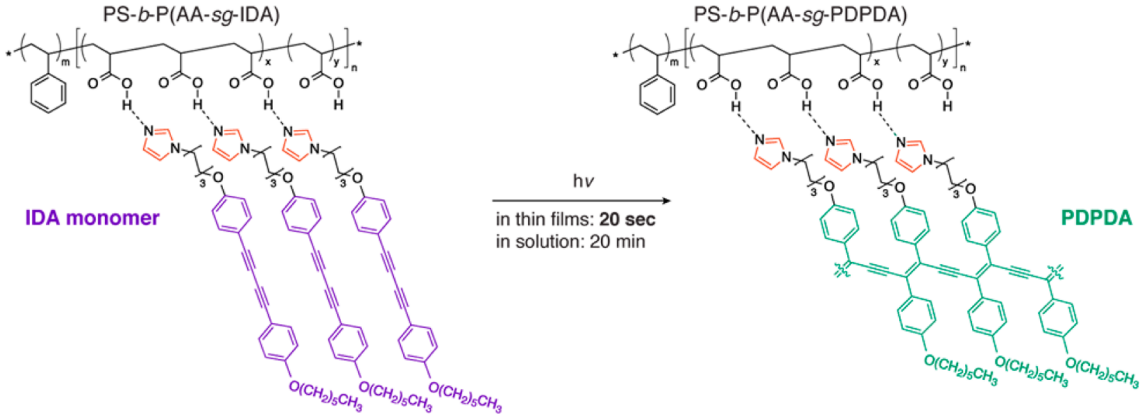

Figure 1. Chemical structures of the block copolymer PS-*b*-PAA, the monomer IDA, and the corresponding polydiacetylene after the BCP-templated photopolymerization of the supramolecular ensemble PS-*b*-(PAA-*sg*-IDA). Note: this is a simplified representation because it is expected that the monomers are randomly distributed along the PAA backbone at IDA:AA ratios less than 1.

based processing by standard techniques with these systems before and after polymerization is difficult due to the lack of molecular preorganization required for the reaction to proceed and the insolubility of the resulting polymers. Therefore, the development of processable and modular solid-state templates for topochemical polymerizations of DAs that do not rely on unpredictable crystal engineering strategies, with fast reactivity (within seconds), are highly desired.[10]

To tackle the various challenges associated with obtaining solution-processable thin films of polydiacetylene by conventional techniques, we employ a BCP[34−37] template-based approach that drastically enhances the topochemical photopolymerization.[38] Additionally, strongly phase segregating BCPs,[39] such as polystyrene-*b*-poly(acrylic acid) (PS-*b*-PAA) templates can be chemically modified to access micropatterns by photolithography, which may be beneficial for the fabrication of multiple devices on a single wafer. Figure 1 shows the supramolecular grafting strategy that exploits strong hydrogen-bonding interactions between the imidazolyl diphenyl-diacetylene (IDA) monomer[40−42] and PS-*b*-PAA. It must be noted that the figure is a simplified representation for the templating strategy. It is not expected that single BCP chains will template single-chain polymerizations of IDA. The supramolecular complex of these two systems is termed PS-*b*-P(AA-*sg*-IDA), where *sg* stands for supramolecular graft of the IDA monomers to the PAA block. This approach takes advantage of the fact that (1) the DPDA moiety has a larger molar extinction coefficient compared to a conventional DA, (2) noncovalent interactions provide modularity to tune the monomer loading ratios, (3) the complexes can be processed from solution by spin-coating, and (4) microphase segregation of the side-chain functional BCPs induces local order that enhances the topochemical polymerization.[21,34,43]

RESULTS AND DISCUSSION

The supramolecular strategy allows for facile tuning of the packing interactions of the IDA monomer by simply varying the molar ratio (R) of the IDA monomer relative to the acrylic acid units along the BCP backbone. The IDA monomer is synthesized in only four steps, and PS-*b*-PAA, which is also commercially available, can be prepared by established procedures.[21] To evaluate the appropriate loading ratio of the monomer, the hydrogen bonding interaction between PS-*b*-PAA and the imidazole group of IDA at various R values

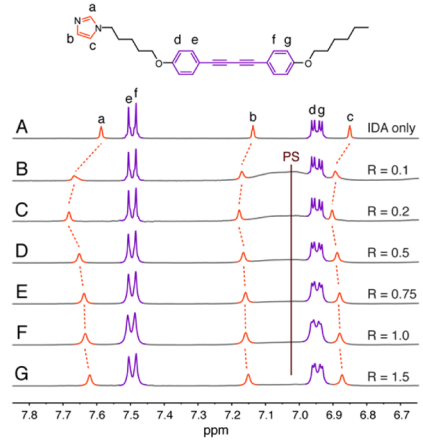

Figure 2. Tuning of the packing interactions by varying the molar ratio. Partial ^{1}H NMR spectra (400 MHz, DMSO-d_6, 298 K) of (A) IDA only and PS-*b*-P(AA-*sg*-IDA) at R = (B) 0.1, (C) 0.2, (D) 0.5, (E) 0.75, (F) 1.0, and (G) 1.5. R = moles of the IDA monomer relative to moles of the acrylic acid units.

(ranging from 0.1 to 1.5) was investigated by proton nuclear magnetic resonance spectroscopy (^{1}H NMR, Figure 2).

As expected, the imidazolyl proton signals broaden upon hydrogen bonding and reach a maximal downfield shift at R = 0.2. By increasing R, the imidazolyl proton signals shift upfield. We attribute these changes to weakened hydrogen bonding interactions between the IDA monomer and PAA, which may be due to steric crowding at high loading.[21] Thus, we focused on loading ratios of R = 0.2 and 0.4 for optimal interactions between the IDA monomers and PAA.

To gauge the importance of the BCP template, photopolymerization of the IDA monomer in solution was studied without PS-*b*-PAA. The IDA monomer was dissolved in chloroform and irradiated with 254 nm for 20 min. Linear absorption and photoluminescence spectra were collected for solutions before and after irradiation (Figure 3A, D). The absorption maxima at 321 and 344 nm, and the emission maxima at 409 and 433 nm, originate from the IDA chromophore. Prolonged irradiation to the solutions resulted in minor spectral changes to both the absorption and photoluminescence spectra, which is indicative that the photopolymerization of the free IDA monomer does not proceed appreciably in solution (Figure 3A,D).

dx.doi.org/10.1021/ja507318u | J. Am. Chem. Soc. 2014, 136, 13381−13387

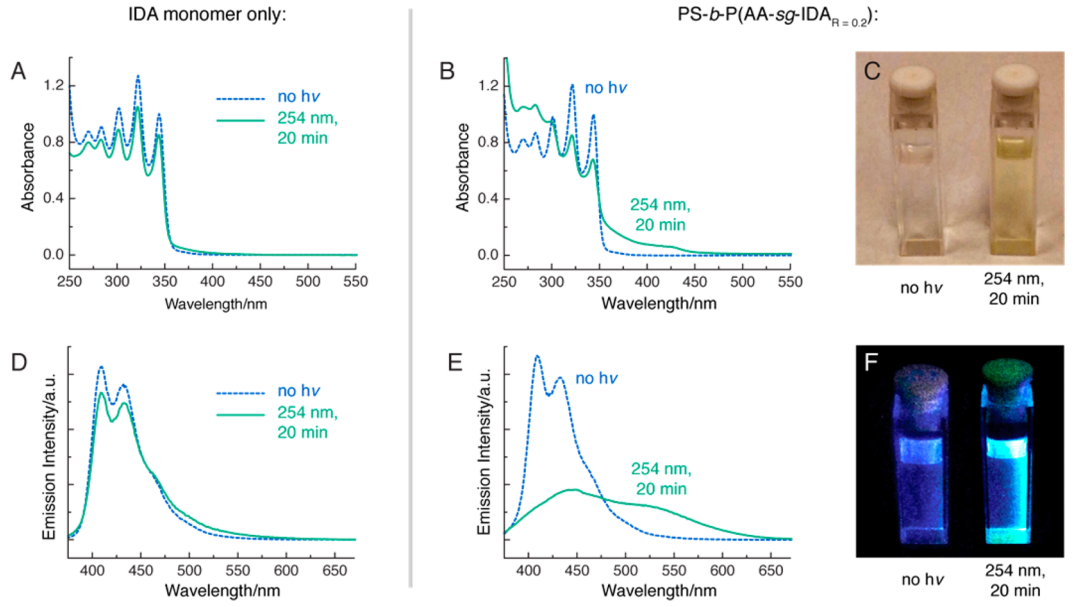

Figure 3. BCP template-based photopolymerization in solution. (A) Absorption spectra of a solution of IDA monomer (dashed line) without irradiation and (solid line) after irradiation at 254 nm for 20 min. (B) Absorption spectra of a solution of PS-*b*-P(AA-*sg*-IDA$_{R=0.2}$) (dashed line) without irradiation and (solid line) after irradiation at 254 nm for 20 min and (C) corresponding image of the solutions under ambient light. (D) Emission spectra (λ_{ex} = 365 nm) of the IDA monomer (dashed line) without irradiation and (solid line) after irradiation at 254 nm for 20 min. (E) Emission spectra (λ_{ex} = 365 nm) of a solution of PS-*b*-P(AA-*sg*-IDA$_{R=0.2}$) (dashed line) without irradiation and (solid line) after irradiation at 254 nm for 20 min and (F) corresponding image of the solutions under a UV light. Spectra were collected at 40 μM of IDA in chloroform at 298 K.

In contrast to the free IDA monomer studies, a reaction of PS-*b*-P(AA-*sg*-IDA$_{R=0.2}$) in solution was observed. This may be analogous to other solution-polymerization studies of DAs, where preassembly of liposomes is required for polymerization to occur[44] or simply from hydrogen-bonded IDA mesogens to the BCPs. But given the observed color changes, we postulate that the yellow color arises from a solvated polydiacetylene, as it has been previously shown in other studies,[45] in addition to unreacted IDA and oligomers in the mixture. In the infrared spectrum of PS-*b*-P(AA-*sg*-PDPDA), the 2208 cm^{-1} vibration appeared due to increased conjugation length along the alternating alkenes and alkynes after photopolymerization. The band at 1630 cm^{-1} became broader by overlapping with the band from the double bonds. (Figure S2, Supporting Information).[45,46] Also, the absorption bands of the IDA monomer in PS-*b*-P(AA-*sg*-IDA$_{R=0.2}$) showed noticeable changes after 20 min of irradiation (Figure 3B)[28,46] with an apparent color change from colorless to pale yellow (Figure 3C). This spectral shift has been observed previously in materials with similar DPDA moieties[45,46] and results from relatively low degrees of polymerization (or oligomerization) coupled with effects from the substituents of DPDA.[47] The most notable change was observed in the photoluminescence spectra, where the 420 nm peak corresponding to the IDA monomer diminished, but did not disappear, after 20 min of irradiation, concomitantly with the appearance of an emission peak near 520 nm corresponding to contributions from PDPDA (Figure 3E, and Figure S3, Supporting Information). Similarly, a change in photoluminescence was observed with λ_{ex} = 365 nm (Figure 3F). Theoretical calculations confirm that the optical transitions of PDPDA are lower in energy than the free IDA monomer and correlate well with the experimentally observed band shift in the simulated absorption spectra (Figures S4 and S5; Tables S1 and S2, Supporting Information). Both absorption and emission spectral variations became saturated after 20 min (Figure S3, Supporting Information). Again, the low photoluminescence peak intensity of PDPDA at 520 nm can be attributed to low degrees of polymerization, given that this system is disordered in solution. Attempts to isolate PDPDA were unsuccessful because of its similar solubility to that of BCP and unreacted IDA monomers. Nonetheless, we postulate that the BCP template led to some alignment for the topochemical reaction of the DA to proceed in solution, though not sufficient for efficient polymerization.

Considering that PS-*b*-P(AA-*sg*-IDA$_{R=0.2}$) is solution-processable, and that microphase segregation of BCPs can enhance molecular alignment through ordered domains,[21,34,43] the photopolymerization was studied in thin films. In addition to organizing the IDA monomers through hydrogen bonding to the PAA backbone, the PS-*b*-PAA template imparts hierarchical order of the IDA monomers through BCP microphase segregation in the solid-state thin films, which is induced by solvent vapor annealing.[47,48] An atomic force microscope (AFM) image of an as-cast film of PS-*b*-P(AA-*sg*-IDA$_{R=0.2}$) displays a featureless surface with roughness ca. 15 nm (Figure 4A). The solvent vapor annealing process was optimized and exposure of the films to DMF for 36 h led to smoother films (roughness ca. 2 nm, compare height scale bar), with a dot-like nanopattern topography resulting from the microphase segregation of PS-*b*-P(AA-*sg*-IDA$_{R=0.2}$) (Figure 4B). Interestingly, a higher loading ratio (R = 0.4) had a subtle enhancement on the packing uniformity of the nanostructure after solvent vapor annealing (Figure 4C,D). Microphase separation of the PS and PAA blocks into roughly spherical domains was observed via high-angle annular dark-field scanning transmission electron microscopy (HAADF-STEM) in both the as-cast materials and the annealed materials (Figure 4E, and Figure S6, Supporting Information). Resolved regions of the lamellar domains attributed to the PDPDA stacks are circled, which are similar to previously reported systems (see GIXRD in

dx.doi.org/10.1021/ja507318u | J. Am. Chem. Soc. 2014, 136, 13381−13387

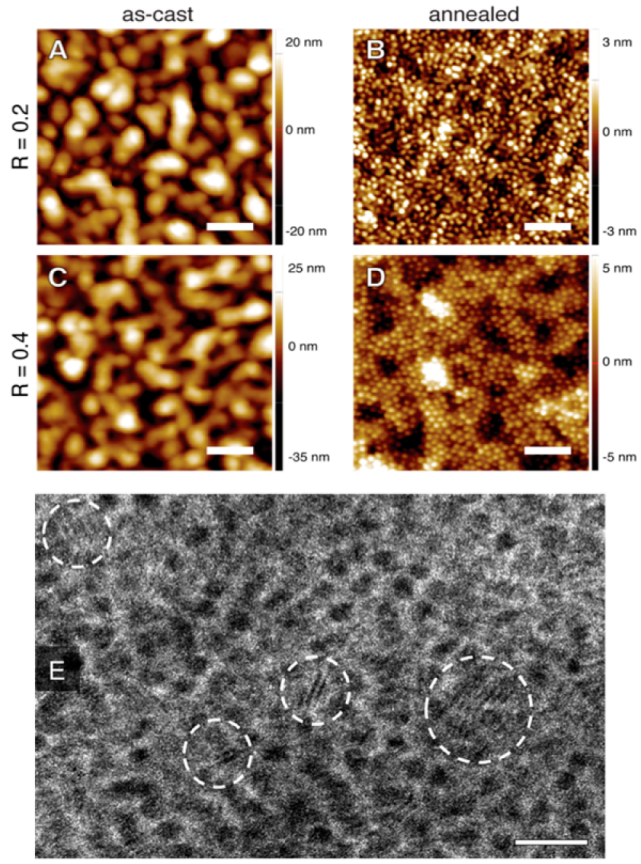

Figure 4. Thin-film self-assembly characterization: AFM topography images of PS-*b*-P(AA-*sg*-IDA$_{R=0.2}$) for an (A) as-cast and (B) solvent-annealed film; AFM topography images of PS-*b*-P(AA-*sg*-IDA$_{R=0.4}$) for an (C) as-cast and (D) solvent-annealed film. (E) HAADF-STEM image of a solvent-annealed film of PS-*b*-P(AA-*sg*-IDA$_{R=0.4}$) after irradiation, where the dark spherical regions correspond to the PS domains. Examples of lamellar crystalline domains are circled. Scale bars are 200 nm and (E) 50 nm.

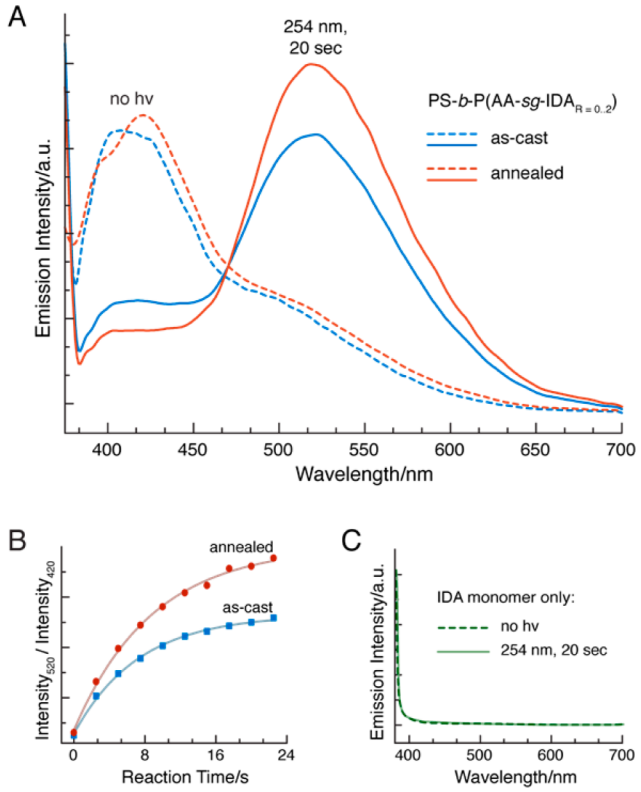

Figure 5. BCP template-based photopolymerization in solid-state thin films. (A) Emission spectra (λ_{ex} = 365 nm) of a thin film of PS-*b*-P(AA-*sg*-IDA$_{R=0.2}$) (dashed line) without irradiation and (solid line) after irradiation at 254 nm for 20 s. The solvent-annealed films (orange) exhibit a higher emission intensity after irradiation when compared to the as-cast films (blue). (B) Time-resolved plots of the intensity at 520 nm (which corresponds to the PDPDA polymer) relative to 420 nm (which corresponds to the IDA monomer) for as-cast films (blue square) and solvent-annealed films (orange circle) of PS-*b*-(PAA-*sg*-IDA$_{R=0.2}$). (C) Emission spectra (λ_{ex} = 365 nm) of a thin film of IDA monomer only (dashed line) without irradiation and (solid line) after irradiation at 254 nm for 20 s.

Figure S6a,b, Supporting Information).[21,49−51] The lamellar crystallite features were only rarely observed in the as-cast sample, indicating that improved organization of the side chains upon annealing facilitated formation of PDPDA lamellar stacks (see Figure S6c−f, Supporting Information).

Relative to templating in solution, significant enhancement of the topochemical polymerization was expected in thin films, where the hierarchical BCP microphase segregation can serve as a handle to align the IDA monomers. In fact, the photopolymerization of PS-*b*-(PAA-*sg*-IDA) in both the as-cast and solvent-annealed thin films was over one order of magnitude faster than in solution. The reaction proceeded within 20 s of UV irradiation, which is the fastest externally triggered reaction time.[28−30,52] Such fast time scales are particularly attractive for high-throughput processing. As compared to the solution reaction (Figure 3E), the photoluminescence spectra of both the as-cast and solvent-annealed thin films display a 420 nm peak corresponding to the IDA monomer that diminished concomitantly with the appearance of a pronounced emission peak near 520 nm, corresponding to PDPDA (Figure 5A). Notably, the intensity of the 520 nm peak is more intense for the thin films, relative to solution, which suggests that the solid-state topochemical photopolymerization of the IDA monomers proceeded to higher degrees of polymerization.

The relative intensity of the 520 nm emission peak corresponding to PDPDA is higher for the solvent-annealed films than the as-cast films (Figure 5A, solid lines). We postulate that BCP microphase segregation further aligns the IDA monomers (Figure 4, and Figure S7, Supporting Information) and enhances the topochemical polymerization, leading to a greater extent of polymerization and resulting in an increased PDPDA emission peak intensity. These differences are more apparent when monitoring the intensity of PDPDA peak relative to emission peak of the IDA monomer with reaction time (I_{520}/I_{420}, Figure 5B, Figure S7, Supporting Information). From this data, the relative photoconversion efficiency can be roughly calculated to be 73% and 80% for the as-cast film and a solvent-annealed film, respectively. As a control experiment, the emission of a thin film of free, non-templated IDA monomer was completely quenched and no spectral changes were observed upon irradiation (Figure 5C). These results indicate that the IDA monomer can be rapidly polymerized to PDPDA using a BCP-templated self-assembled morphology in the solid state, which induces the appropriate alignment of IDA monomers.

Given the fast and efficient photopolymerization observed with this BCP-templated system, we sought to investigate

dx.doi.org/10.1021/ja507318u | J. Am. Chem. Soc. 2014, 136, 13381−13387

photopatterning strategies to generate hierarchical shapes at the micrometer length scale. Thin films of PS-*b*-P(AA-*sg*-IDA) are soluble in common solvents. Hence, 4-bromostyrene (BrS) was incorporated, yielding P(S-*co*-BrS)-*b*-PAA, which simultaneously cross-links during photopolymerization at 254 nm (Figure 6A,B).[53,54] Solvent-annealed thin films of P(S-*co*-BrS)-*b*-P(AA-*sg*-IDA) exhibit comparable microphase-segregated nanostructures as PS-*b*-P(AA-*sg*-IDA) (Figure S8, Supporting Information). Through standard shadow-mask photolithography, micropatterns of the hierarchical solvent-annealed thin films of P(S-*co*-BrS)-*b*-(PAA-*sg*-PDPDA) were fabricated and visualized using confocal microscopy in the 510−530 nm channel, which corresponds to emission from PDPDA (Figure 6C, and Figure S9, Supporting Information). The faint background fluorescence in Figure 6C may arise from light leakage through the shadow mask, because this process was carried out on a benchtop setup without the traditional automated mask aligner. Moreover, confocal microscopy imaging in the 460−480 nm channel shows that the IDA monomer is readily consumed, and the faint signal can be attributed to contributions from the PDPDA and the IDA monomer. In this system, the combination of cross-linkable templates and self-assembly has enabled us to fabricate thin films of micropatterned PDPDA, a strategy that could be useful for the fabrication of microarrays of conjugated photoluminescent materials.

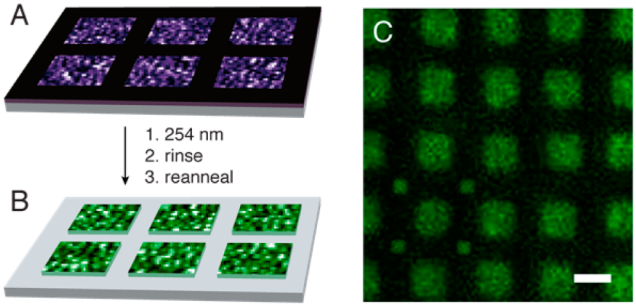

Figure 6. Photopatterning experiments. (A) Solvent-annealed thin films of P(S-*co*-BrS)-*b*-P(AA-*sg*-IDA) are aligned with a shadow mask and cross-linked with 254 nm. (B) After a rinse and reannealing step, hierarchical patterns are achieved, (C) as observed by confocal microscopy in the 510−530 nm channel. Scale bar is 500 μm.

CONCLUSION

The BCP-templated strategy described here has enabled us to efficiently drive the topochemical polymerization of a diphenyl diacetylene derivative (IDA) in solution and thin films. It is important to note that common strategies rely on crystal engineering and/or stringent supramolecular recognition design, which can be challenging to control in a predictable fashion. The viability of our approach is rooted not only in processability and modularity but also on the facile synthesis of the materials. Hydrogen-bonding interactions between imidazole on the IDA monomer and the acrylic acid on the BCP template provided effective molecular alignment that led to rapid photochemical polymerization to synthesize a supramolecularly grafted PDPDA. Moreover, the microphase-segregated structure arising from the BCP further improves the organization of the IDA monomers, which led to the solid-state, BCP-templated polymerization. Notably, the topochemical reaction can be completed within tens of seconds. Exploiting such rapid reactivity, we fabricated micropatterns by photolithography through the simultaneous cross-linking of 4-bromostyrene-functional BCP thin films during photopolymerization. Future studies will be geared toward exploiting this templated supramolecular grafting strategy, which could be useful in other topochemical reactions that require highly uniform molecular alignment.

EXPERIMENTAL SECTION

General. ^{1}H NMR and ^{13}C NMR spectra were measured on a Bruker 400 MHz spectrometer. The fast atom bombardment (FAB) mass spectra and high-resolution mass spectrometry (HR-MS) were recorded on a JMS-HX110 HF mass spectrometer (ionization mode: FAB+). Absorption spectra were recorded on a Shimadzu 1800 spectrophotometer, and the photoluminescence emission spectra were collected with a Jobin Yvon Fluorolog-3 spectrofluorometer (Model FL-TAU3). The photoirradiation was carried on PL Series compact UV lamp (4 W) with an irradiation wavelength of 254 nm. The distance between the lamp and the sample was kept within 3−5 cm. Argon bubbling was applied upon the irradiation of those solution samples. Infrared spectra were obtained using a PerkinElmer Spectrum400 FTIR spectrometer using a PIKE ATR attachment. The atomic force microscopy images were collected on a Park System PSI XE100 atomic force microscope. Thermal gravimetric analysis was conducted with a TA Instruments Q50. The thickness of thin films was determined with a Rudolph EL III ellipsometer. Transmission electron microscopy was performed on a JEOL JEM-2100F field emission TEM at 200 kV. High-angle annular dark-field (HAADF) STEM images were collected using a Gatan Model 806 HAADF-STEM detector with a 40 μm condenser aperture, 2 cm camera length, and 0.5 nm spot size. Data analysis was performed using Gatan Digital Micrograph 3 software. The fluorescence images were captured by a LEICA TCS SP5 confocal microscope.

See Supporting Information for the scheme pertaining to the compound labels below.

Synthesis of Compound 1. Compound **1** was prepared according to a similar procedure described in the literature.[55]

Synthesis of Compound 2. A solution of hexyl bromide (1.05 g, 6.36 mmol) in anhydrous acetone (5 mL) was added dropwise into a mixture of compound **1** (1.5 g, 6.41 mmol) and potassium carbonate (0.8 g, 5.8 mmol) in anhydrous acetone (15 mL) at 60 °C. The mixture was stirred for 12 h at 60 °C under Ar. The solvent was removed in vacuo, and the residue was purified by silica gel chromatography (hexane/ethyl acetate = 6:1) to afford gray compound **2** (1.02 g, 50.4%). ^{1}H NMR (400 MHz, $CDCl_3$, 298 K): δ = 7.45 (d, J = 9.2 Hz, 2H), 7.42 (d, J = 8.8 Hz, 2H), 6.84 (d, J = 8.8 Hz, 2H), 6.79 (d, J = 8.8 Hz, 2H), 3.97 (t, J = 6.4 Hz, 2H), 1.79 (m, 2H), 1.46 (m, 2H), 1.35 (m, 4H), 0.91 (t, J = 7.2 Hz, 3H). ^{13}C NMR (100 MHz, $CDCl_3$, 298 K): δ = 159.91, 156.32, 134.29, 134.06, 115.66, 114.68, 114.36, 113.62, 81,43, 81.00, 73.01, 72.82, 68.25, 31.57, 29.18, 25.76, 22.60, 14.04. MS (FAB+): calcd for $[M]^+$ m/z = 318.2, found m/z: 318.3; HR-MS (FAB+): calcd for $C_{22}H_{22}O_2$ $[M]^+$ m/z = 318.1620, found m/z: 318.1619.

Synthesis of Compound 3. Compound **2** (0.6 g, 1.89 mmol) was added to 1,6-dibromohexane (4.5 g, 18.4 mmol) in acetone (5 mL). Potassium carbonate (520 mg, 3.77 mmol) was added and the mixture refluxed for 6 h under Ar protection. The solution was filtered, and the filtrate was precipitated in a 4-fold volume of hexane. The solid was filtered, washed with petroleum (30 mL) and deionized water (20 mL), and dried under vacuum to obtain gray compound **3** (737 mg, 81.1%). ^{1}H NMR (400 MHz, $CDCl_3$, 298 K): δ = 7.44 (d, J = 8.0 Hz, 4H), 6.83 (d, J = 7.6 Hz, 4H), 3.97 (m, 4H), 3.42 (t, J = 6.8 Hz, 2H), 1.90 (m, 2H), 1.81 (m, 4H), 1.50 (m, 6H), 1.34 (m, 4H), 0.91 (t, J = 6.8 Hz, 3H). ^{13}C NMR (100 MHz, $CDCl_3$, 298 K): δ = 159.89, 159.74, 134.04, 134.04, 114.66, 114.64, 113.85, 113.67, 81,38, 81.27, 72.97, 72.89, 68.17, 67.86, 33.79, 32.66, 31.56, 29.13, 28.99, 27.91, 25.69, 25.28, 22.61, 14.03. MS (FAB+): calcd for $[M]^+$ m/z = 480.2 (^{79}Br), found m/z: 480.2 (^{79}Br); HR-MS (FAB+): calcd for $C_{28}H_{33}O_2{}^{79}Br$ $[M]^+$ m/z = 480.1664, found m/z: 480.1668.

dx.doi.org/10.1021/ja507318u | J. Am. Chem. Soc. 2014, 136, 13381−13387

Synthesis of IDA. To a mixture of compound **3** (650 mg, 1.35 mmol) and potassium hydroxide (151 mg, 2.78 mmol) in acetonitrile (6 mL) was added imidazole (645 mg, 9.48 mmol). The reaction mixture was refluxed for 8 h and then cooled to room temperature. After flash column chromatography (ethyl acetate/methanol = 25:2), the crude product was washed with deionized water (15 mL) and dried under vacuum to obtain pure white compound IDA (255 mg, 40.4%). ^{1}H NMR (400 MHz, $CDCl_3$, 298 K): δ = 7.46 (s, 1H), 7.44 (d, J = 8.4 Hz, 4H), 7.06 (s, 1H), 6.91 (s, 1H), 6.84 (d, J = 8.8 Hz, 2H), 6.81 (d, J = 8.4 Hz, 2H), 3.96 (m, 6H), 1.78 (m, 6H), 1.47 (m, 4H), 1.34 (m, 6H), 0.91 (t, J = 6.8 Hz, 3H). ^{13}C NMR (100 MHz, $CDCl_3$, 298 K): δ = 159.90, 159.67, 137.10, 134.04, 134.04, 129.50, 118.77, 114.67, 114.62, 113.91, 113.65, 81,42, 81.21, 73.01, 72.87, 68.16, 67.72, 46.94, 31.56, 31.03, 29.12, 28.97, 26.34, 25.69, 25.62, 22.60, 14.03. MS (FAB+): calcd for $[M + H]^+$ m/z = 469.3, found m/z: 469.4; HR-MS (FAB+): calcd for $C_{31}H_{37}O_2N_2$ $[M + H]^+$ m/z = 469.2855, found m/z: 469.2860.

Synthesis of PS-b-PAA and P(S-co-BrS)-b-PAA. PS(7K)-*b*-PAA-(8.1K) was synthesized by reversible addition−fragmentation chain transfer (RAFT) according to previously reported literature.[21] Likewise, P[S(5.4K)-*co*-BrS(0.7K)]-*b*-PAA(8.1K) was synthesized by RAFT with 10 mol % incorporation of BrS.

Computational Details. Theoretical calculations were carried out using the Gaussian 09 program package.[56] The geometries of the monomer model and the diacetylene model were optimized by density functional theory (DFT) calculations, using the hybrid B3LYP functional[57] and the 6-31G* basis set.[58] At the optimized geometries, time-dependent (TD) DFT calculations were performed using the range-separated hybrid CAM-B3LYP functional,[59] with solvent effects of chloroform taken into account by the polarizable continuum model (PCM).[60]

Thin-Film Preparation. Solutions of PS-*b*-P(AA-*sg*-IDA) (6 mM in dioxane) were spin-coated (2500 rpm, 45 s) on silicon chips. The thicknesses of the films were 60−70 nm. The chips were inserted into the cuvette holder with an angle about ∼45° to the incident light for the optical tests.

Solvent Annealing. Solvent vapor annealing was optimized by varying the solvent (toluene, benzene, chloroform, acetone, THF, dioxane, and DMF) and annealing time (0.5 h, 1 h, 2 h, 4 h, 12 h, 36 h, and 72 h). Thin films were analyzed by AFM. We found that the optimal solvent vapor annealing conditions for our system involves annealing in a 200 mL closed jar with DMF vapor for 36 h.

Photopatterning. A quartz mask with micron-sized chromium patterns was aligned to the thin films in a nitrogen atmosphere. Irradiation at 254 nm for 20 s afforded the cross-linked thin films and polymerized the IDA monomers. Then the films were washed with dioxane 3× and dried with a nitrogen stream. The micropatterns were imaged with confocal microscopy, using different wavelength channels, where the intensity of each channel was read under the same gain.

■ ASSOCIATED CONTENT

Ⓢ Supporting Information

Complementary characterization data, figures, and computational results. This material is available free of charge via the Internet at http://pubs.acs.org.

■ AUTHOR INFORMATION

Corresponding Authors

kathryn.l.killops.civ@mail.mil
lcampos@columbia.edu

Notes

The authors declare no competing financial interest.

■ ACKNOWLEDGMENTS

This research was funded by the Department of the Army Basic Research Program and sponsored by the Edgewood Chemical Biological Center. Financial support for L.Z. was provided by the Army Research Office under award number W911NF-12-1-0252. The self-assembly characterization was funded by an NSF CAREER grant (DMR-1351293). H.T. thanks the Department of Defense (DOD) for the National Defense Science & Engineering Graduate (NDSEG) Fellowship. K.L.K. thanks the Army Basic Research Program for funding. We thank Dr. J. Xia and Dr. S. Wei for helpful discussions and D. Hanifi for the assistance with the GISAXS studies.

■ REFERENCES

(1) Green, M. A. *Prog. Photovoltaics* **2001**, *9*, 123.
(2) Ito, H.; Willson, C. G. *Polym. Eng. Sci.* **1983**, *23*, 1012.
(3) Jung, B.; Satish, P.; Bunck, D. N.; Dichtel, W. R.; Ober, C. K.; Thompson, M. O. *ACS Nano* **2014**, *8*, 5746−5756.
(4) Campos, L. M.; Garcia-Garibay, M. A. In *Reviews of Reactive Intermediate Chemistry*; Platz, M. S., Moss, R. A., Maitland Jones, J., Eds.; John Wiley & Sons, Inc.: Hoboken, NJ, 2007; p 271.
(5) Leibfarth, F. A.; Kang, M.; Ham, M.; Kim, J.; Campos, L. M.; Gupta, N.; Moon, B.; Hawker, C. J. *Nat. Chem.* **2010**, *2*, 207.
(6) Leibfarth, F. A.; Wolffs, M.; Campos, L. M.; Delany, K.; Treat, N.; Kade, M. J.; Moon, B.; Hawker, C. J. *Chem. Sci.* **2012**, *3*, 766.
(7) Campos, L. M.; Dang, H.; Ng, D.; Yang, Z.; Martinez, H. L.; Garcia-Garibay, M. A. *J. Org. Chem.* **2002**, *67*, 3749.
(8) Toda, F. *Acc. Chem. Res.* **1995**, *28*, 480.
(9) Ramamurthy, V.; Venkatesan, K. *Chem. Rev.* **1987**, *87*, 433.
(10) Dou, L.; Zheng, Y.; Shen, X.; Wu, G.; Fields, K.; Hsu, W.-C.; Zhou, H.; Yang, Y.; Wudl, F. *Science* **2014**, *343*, 272.
(11) Meng, H.; Perepichka, D. F.; Bendikov, M.; Wudl, F.; Pan, G. Z.; Yu, W.; Dong, W.; Brown, S. *J. Am. Chem. Soc.* **2003**, *125*, 15151.
(12) Lauher, J. W.; Fowler, F. W.; Goroff, N. S. *Acc. Chem. Res.* **2008**, *41*, 1215.
(13) Colson, J. W.; Dichtel, W. R. *Nat. Chem.* **2013**, *5*, 453.
(14) Inokuma, Y.; Kawano, M.; Fujita, M. *Nat. Chem.* **2011**, *3*, 349.
(15) Xu, L.-P.; Yan, C.-J.; Wan, L.-J.; Jiang, S.-G.; Liu, M.-H. *J. Phys. Chem. B* **2005**, *109*, 14773.
(16) Chan, Y.-H.; Lin, J.-T. s.; Chen, I. W. P.; Chen, C.-h. *J. Phys. Chem. B* **2005**, *109*, 19161.
(17) Lu, Y.; Yang, Y.; Sellinger, A.; Lu, M.; Huang, J.; Fan, H.; Haddad, R.; Lopez, G.; Burns, A. R.; Sasaki, D. Y.; Shelnutt, J.; Brinker, C. J. *Nature* **2001**, *410*, 913.
(18) Sun, A.; Lauher, J. W.; Goroff, N. S. *Science* **2006**, *312*, 1030.
(19) Cohen, M. J.; Garito, A. F.; Heeger, A. J.; MacDiarmid, A. G.; Mikulski, C. M.; Saran, M. S.; Kleppinger, J. *J. Am. Chem. Soc.* **1976**, *98*, 3844.
(20) Hasegawa, M. In *Advances in Physical Organic Chemistry*; Bethell, D., Ed.; Academic Press: New York, 1995; Vol. *30*, p 117.
(21) Tran, H.; Gopinadhan, M.; Majewski, P. W.; Shade, R.; Steffes, V.; Osuji, C. O.; Campos, L. M. *ACS Nano* **2013**, *7*, 5514.
(22) Wegner, G. *Z. Naturforsch.* **1969**, *246*, 824.
(23) Kraabel, B.; Hulin, D.; Aslangul, C.; Lapersonne-Meyer, C.; Schott, M. *Chem. Phys.* **1998**, *227*, 83.
(24) McQuade, D. T.; Pullen, A. E.; Swager, T. M. *Chem. Rev.* **2000**, *100*, 2537.
(25) Xu, Q.; Lee, S.; Cho, Y.; Kim, M. H.; Bouffard, J.; Yoon, J. *J. Am. Chem. Soc.* **2013**, *135*, 17751.
(26) Diegelmann, S. R.; Tovar, J. D. *Macromol. Rapid Commun.* **2013**, *34*, 1343.
(27) Pope, M.; Swenberg, C. E. *Electronic Processes in Organic Crystals and Polymers*, 2nd ed.; Oxford University Press: New York, 1999.
(28) Kim, J.-H.; Lee, E.; Jeong, Y.-H.; Jang, W.-D. *Chem. Mater.* **2012**, *24*, 2356.
(29) Sun, X.; Chen, T.; Huang, S.; Li, L.; Peng, H. *Chem. Soc. Rev.* **2010**, *39*, 4244.
(30) Yoon, B.; Lee, S.; Kim, J.-M. *Chem. Soc. Rev.* **2009**, *38*, 1958.
(31) Xu, W. L.; Smith, M. D.; Krause, J. A.; Greytak, A. B.; Ma, S.; Read, C. M.; Shimizu, L. S. *Cryst. Growth Des.* **2014**, *14*, 993.
(32) Xu, Y.; Smith, M. D.; Geer, M. F.; Pellechia, P. J.; Brown, J. C.; Wibowo, A. C.; Shimizu, L. S. *J. Am. Chem. Soc.* **2010**, *132*, 5334.

(33) Diegelmann, S. R.; Hartman, N.; Markovic, N.; Tovar, J. D. *J. Am. Chem. Soc.* **2012**, *134*, 2028.
(34) Bates, F. S.; Fredrickson, G. H. *Phys. Today* **1999**, *52*, 32.
(35) Eugene, D. M.; Grayson, S. M. *Macromolecules* **2008**, *41*, 5082.
(36) Sai, H.; Tan, K. W.; Hur, K.; Asenath-Smith, E.; Hovden, R.; Jiang, Y.; Riccio, M.; Muller, D. A.; Elser, V.; Estroff, L. A.; Gruner, S. M.; Wiesner, U. *Science* **2013**, *341*, 530.
(37) Tavakkoli, K. G. A.; Gotrik, K. W.; Hannon, A. F.; Alexander-Katz, A.; Ross, C. A.; Berggren, K. K. *Science* **2012**, *336*, 1294.
(38) Patel, G. N.; Chance, R. R.; Turi, E. A.; Khanna, Y. P. *J. Am. Chem. Soc.* **1978**, *100*, 6644.
(39) Kempe, K.; Killops, K. L.; Poelma, J. E.; Jung, H.; Bang, J.; Hoogenboom, R.; Tran, H.; Hawker, C. J.; Schubert, U. S.; Campos, L. M. *ACS Macro Lett.* **2013**, *2*, 677.
(40) Arakawa, Y.; Nakajima, S.; Kang, S.; Konishi, G.-i.; Watanabe, J. *J. Mater. Chem.* **2012**, *22*, 14346.
(41) Kim, Y.; Shin, S.; Kim, T.; Lee, D.; Seok, C.; Lee, M. *Angew. Chem., Int. Ed.* **2013**, *52*, 6426.
(42) Wu, S.-T.; Margerum, J. D.; Meng, H. B.; Dalton, L. R.; Hsu, C. S.; Lung, S. H. *Appl. Phys. Lett.* **1992**, *61*, 630.
(43) Gopinadhan, M.; Majewski, P. W.; Beach, E. S.; Osuji, C. O. *ACS Macro Lett.* **2012**, *1*, 184.
(44) Okada, S.; Peng, S.; Spevak, W.; Charych, D. *Acc. Chem. Res.* **1998**, *31*, 229.
(45) Schott, M. *J. Phys. Chem. B* **2006**, *110*, 15864.
(46) Wiley, R. H.; Lee, J. Y. *J. Macromol. Sci., Chem.* **1971**, *5*, 513.
(47) Krishnamoorthy, S.; Hinderling, C.; Heinzelmann, H. *Mater. Today* **2006**, *9*, 40.
(48) Tang, C.; Lennon, E. M.; Fredrickson, G. H.; Kramer, E. J.; Hawker, C. J. *Science* **2008**, *322*, 429.
(49) Deshmukh, P.; Ahn, S.-k.; Geelhand de Merxem, L.; Kasi, R. M. *Macromolecules* **2013**, *46*, 8245.
(50) Majewski, P. W.; Gopinadhan, M.; Jang, W.-S.; Lutkenhaus, J. L.; Osuji, C. O. *J. Am. Chem. Soc.* **2010**, *132*, 17516.
(51) Mao, G.; Wang, J.; Clingman, S. R.; Ober, C. K.; Chen, J. T.; Thomas, E. L. *Macromolecules* **1997**, *30*, 2556.
(52) Sun, X.; Chen, T.; Huang, S.; Cai, F.; Chen, X.; Yang, Z.; Li, L.; Cao, H.; Lu, Y.; Peng, H. *J. Phys. Chem. B* **2010**, *114*, 2379.
(53) Kern, W.; Hobisch, J.; Hummel, K. *Macromol. Chem. Phys.* **1997**, *198*, 3987.
(54) Kumar, K.; Luchnikov, V.; Nandan, B.; Senkovskyy, V.; Stamm, M. *Eur. Polym. J.* **2008**, *44*, 4115.
(55) Park, J.; Park, E.; Kim, A.; Park, S. A.; Lee, Y.; Chi, K. W.; Jung, Y. H.; Kim, I. S. *J. Org. Chem.* **2011**, *76*, 2214.
(56) Frisch, M. J.; Trucks, G. W.; Schlegel, H. B.; Scuseria, G. E.; Robb, M. A.; Cheeseman, J. R.; Scalmani, G.; Barone, V.; Mennucci, B.; Petersson, G. A.; et al. *Gaussian 09, Revision A.2*, Gaussian, Inc., Wallingford, CT, 2009.
(57) Becke, A. D. *J. Chem. Phys.* **1993**, *98*, 5648.
(58) Hehre, W. J. *J. Chem. Phys.* **1972**, *56*, 2257.
(59) Yanai, T.; Tew, D. P.; Handy, N. C. *Chem. Phys. Lett.* **2004**, *393*, 51.
(60) Tomasi, J.; Mennucci, B.; Cammi, R. *Chem. Rev.* **2005**, *105*, 2999.